Multiphysics modeling of a rail gun launcher

Y. W. Kwon, N. Pratikakis, and M. R. Shellock
Dept. of Mechanical and Astronautical Engineering
Naval Postgraduate School Monterey, CA 93943 USA

ABSTRACT

A finite element based multiphysics modeling was conducted for a rail gun launcher to predict the exit velocity of the launch object, and temperature distribution. For this modeling, electromagnetic field analysis, heat transfer analysis, thermal stress analysis, and dynamic analysis were conducted for a system consisting of two parallel rails and a moving armature. In particular, an emphasis was given to model the contact interface between rails and the armature. A contact theory was used to estimate the electric as well as thermal conductivities at the interface. Using the developed model, a parametric study was conducted to understand effects of various parameters on the exit velocity as well as the temperature distribution in the rail gun launcher.

1. INTRODUCTION

The rail gun is a type of projectile weapon [1]. The basic structure of the rail gun is depicted in Fig. 1. It is so named because it consists of twin rails and it is a device to accelerate a projectile to a high speed in a short time using electromagnetic force. A large current is sent out along one of two parallel conducting rails, across a conducting armature between the rails, and then back to the current source along the second rail. The projectile to be fired lies on the far side of the armature and fits loosely between the rails. The currents in the rails produce magnetic fields between the rails. The net magnetic field exerts a force on the armature due to the current that goes through it. The force points outward along the rails and pushes the projectile, accelerating and launching it at a very high velocity. There are different types of rail guns to enhance the launch power. One is made of a solid armature, and another one is constructed of plasma armature. In addition, there are series-augmented rails or parallel-augmented rails.

There have been many researches conducted for rail guns [2–6]. Because the electromagnetic field is the major player of rail guns, most of research was performed to analyze electromagnetic fields. Various formulations have been developed to determine the electromagnetic solutions of moving conductors [7–14]. The majority of them used the finite element method while some others used the boundary element method [13] and the coupled finite and boundary element method [10]. In addition, a parallel algorithm was presented [14].

Some of the research also investigated coupled problems, mostly electromagnetic and thermal analyses together [2,9] because electric current generates heat. This is also an important aspect in a rail gun. However, to the authors' best knowledge, the contact interface

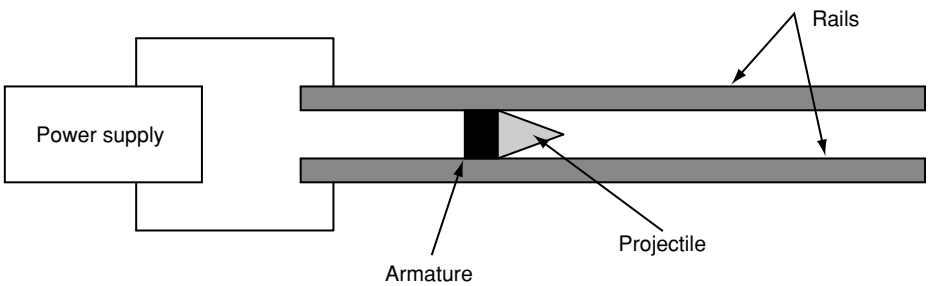

Figure 1 Basic structure of a rail gun.

conditions between two conductors, such as an armature and a rail, have been neglected in previous studies even though those conditions affect the electromagnetic as well as thermal fields significantly. As a result, the present paper developed a multiphysics based modeling technique of a rail gun launcher using the finite element method.

In this study, a multiphysics modeling was conducted for a rail gun launcher to predict the exit velocity of the launch object and temperature distribution. For this modeling, electromagnetic field analysis, heat transfer analysis, thermal stress analysis, and dynamic analysis were conducted for a system consisting of two parallel rails and a moving armature. Especially, a contact theory was used to estimate the electric as well as thermal conductivities at the interface.

The following sections present mathematical models for multiphysics analyses, a contact theory for electric and thermal conductivities at the contact interfaces, and results and discussion followed by conclusions.

2. MATHEMATICAL MODELS FOR MULTIPHYSICS ANALYSES

The present analysis of a rail gun launcher is based on a multiphysics finite element model. The overall schematic of the analyses is sketched in Fig. 2 and described below. The whole analysis was a time-dependent problem. Starting with the initial position of the armature between two rails, electromagnetic wave analysis was first conducted. From that analysis, the Lorentz force, which is the driving force of the armature and the projectile, was calculated. Then, heat generation was computed from Joule's law, and transient heat transfer analysis was undertaken. Using the temperature distribution, thermal stress analysis was performed and the contact load wass computed between the armature and the rails. Finally, by applying Newton's second law to the armature with Lorentz force and friction force between the armature and rails, the acceleration of the armature was determined. First and second integrations of the acceleration over the time increment resulted in velocity and position of the armature. If the armature was still inside the parallel rails, the whole analysis repeated itself. Otherwise, the program wais terminated and the exit velocity was determined.

The interface electric and thermal conductivities between the armature and rails contribute significantly to the electromagnetic field and temperature field. As a result, it was necessary to estimate those properties accurately. In order to determine those interface properties, a contact model was also applied. Each analysis is described in more detail subsequently.

The whole analysis process began with electromagnetic field analysis. For the electromagnetic field analysis, the finite element method was applied to Maxwell's equations which are written below

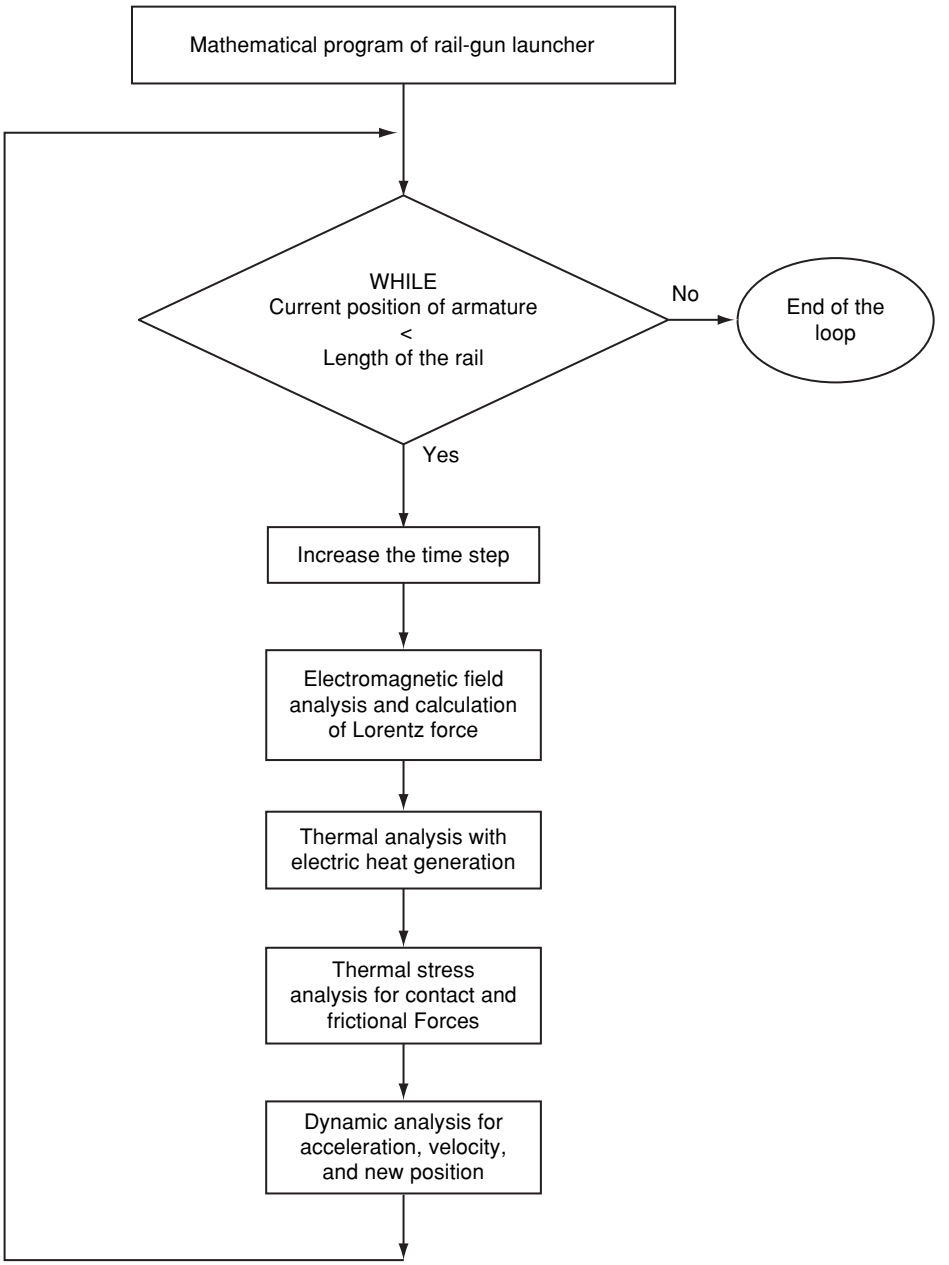

Figure 2 Schematic representation of the overall computer program.

$$\nabla \times \vec{\mathrm{H}} = \vec{J} \tag{1}$$

$$\nabla \times \vec{E} = -\frac{\vec{\partial} B}{\partial t} \tag{2}$$

$$\nabla \times \vec{B} = 0 \tag{3}$$

$$\nabla \times \vec{J} = 0 \tag{4}$$

where $\vec{H}$ is the magnetic field intensity vector, $\vec{J}$ is the current density vector, $\vec{E}$ is the electric field intensity vector, and $\vec{B}$ is the magnetic flux vector. The electromagnetic field of the rail gun launcher is dependent on the electric conductivity at the interface between the armature and rails. So as to estimate the electric conductivity, a fractal based contact model was adopted, which is described in the next section.

Once the electromagnetic field was computed from the equations, the Lorentz force was computed for the electrically conducting armature. Furthermore, Joule's law was applied to calculate heat generation as shown below:

$$Q = \frac{\left|\vec{J}\right|^2}{\sigma} \tag{5}$$

in which σ is the electric conductivity.

From the electrical heat generation, thermal analysis was conducted using the following transient heat conduction equation

$$\nabla \cdot (k \nabla T) + Q = C_p \frac{\partial T}{\partial t} \tag{6}$$

where T is temperature, k is thermal conductivity and C_p is specific heat of the materials. The heat transfer in the launcher is also affected by the contact interface. Therefore, the same contact model used for electric conductivity at the interface was also utilized for thermal conductivity at the interface.

Using the temperature distribution in the launcher, thermal stress analysis was undertaken using the following set of equations. The stress equilibrium for 2-D is expressed as

$$\frac{\partial \tau_{xx}}{\partial x} + \frac{\partial \tau_{xy}}{\partial y} = 0 \tag{7}$$

and

$$\frac{\partial \tau_{xy}}{\partial x} + \frac{\partial \tau_{yy}}{\partial y} = 0 \tag{8}$$

where τ_{ij} is the stress tensor. Stresses and strains are related for an isotropic material using generalized Hooke's law as given below:

$$\varepsilon_{xx} = \frac{1}{Y}(\tau_{xx} - v\tau_{yy}) + \alpha T \tag{9}$$

$$\varepsilon_{yy} = \frac{1}{Y}(\tau_{yy} - v\tau_{xx}) + \alpha T \tag{10}$$

$$\varepsilon_{xy} = \frac{1}{2G}\tau_{xy} \tag{11}$$

where ε_{ij} is the strain tensor, Y is the elastic modulus, G is the shear modulus, v is Poisson's ratio, and α is the coefficient of thermal expansion. Finally, the strain-displacement relationship is written as

$$\varepsilon_{xx} = \frac{\partial u}{\partial x} \tag{12}$$

$$\varepsilon_{yy} = \frac{\partial v}{\partial y} \tag{13}$$

$$2\varepsilon_{xy} = \frac{\partial u}{\partial y} + \frac{\partial v}{\partial x} \tag{14}$$

where u and v are the displacements in the x and y directions, respectively.

Equations (7) through (14) were solved using the finite element method with a known temperature field [15]. From the stress analysis, the contact force between the armature and the rails was computed. Then, using Coulomb's frictional law, the frictional force at the interface was calculated. Eventually, the net force was determined by subtracting the frictional force from the Lorentz force. Using the net force, dynamic analysis was performed to find the acceleration of the armature by applying Newton's second law. Time integration of the acceleration yielded velocity, and another time integration of the velocity resulted in the new position of the armature. The Euler integration scheme was utilized for time integration. As long as the armature was still in contact with the rails, the whole analysis starting from electromagnetic analysis to dynamic analysis was repeated.

3. CONTACT MODEL

As the armature and rails are in contact, electricity and heat pass through the contact surfaces. Therefore, both electric and thermal conductivities of the contact interface play an important role in the electromagnetic and temperature fields, which also affect the projectile exit velocity. In order to estimate thermal or electric conductivity (or resistivity) at the contact interface, a fractal surface contact model [16] was adopted in this research. A nominally flat surface has a surface roughness such as peaks and valleys at the small length scale. When two nominally flat surfaces meet each other, those peaks and valleys are encountered one another as actual contacts. As a result, the nominal contact interface consists of the actual contact area and the void area. The void area usually contains air which has much less conductivities compared to metallic materials. For hear transfer, there is a radiation in the void. However, this effect was also neglected. Therefore, overall conductivities of the interface depend on the amount of actual contact area.

The roughness of a nominally flat surface (i.e. peaks and valleys) was constructed using a fractal model. The first step in modeling the fractal surface was to use the following fractal surface equation developed by Yan and Komvopoulos [16]:

$$z(x,y) = L\left(\frac{G}{L}\right)^{(D-2)}\left(\frac{\ln\gamma}{M}\right)^{1/2}\sum_{m=1}^{M}\sum_{n=0}^{n_{\max}}\gamma^{(D-3)n} \times \left\{\cos\phi_{m,n} - \cos\left[\frac{2\pi\gamma^{n}\left(x^{2}-y^{2}\right)^{1/2}}{L} \times \cos\left(\tan^{-1}\left(\frac{y}{x}\right) - \frac{\pi m}{M}\right) + \phi_{m,n}\right]\right\} \quad (15)$$

In this equation, M indicates the number of superposed fractal ridges, G is called fractal roughness, D is the fractal dimension, γ is the density of the profile frequency, L and ϕ are length and angle parameters, and $n_{\max}$ is the number of summation. The following parameters were used as the baseline as used in Ref. [16]:

L	=	1.0×10^{-8} (m)	γ	=	1.5	ϕ	= 5.9698 (rad)
G	=	1.36×10^{-11} (m)	M	=	10		
D	=	1.2	$n_{\max}$	=	100		

Figure 3 shows the fractal surface generated from the above equation and selected parameters.

A computer code was then developed to determine the locations of local peaks of the plotted fractal surface. A peak was defined as a specific point whose value for z was larger than both the preceding and following value of z in the x and y directions. The height of the peak, or z value, was then saved into a column vector for further calculations. Using this column vector, the peak radius was solved for at each location deemed a peak. To solve for the peak radius, the radius of curvature at the location of the peak was computed. This was computed by setting the radius of curvature equal to the reciprocal of the second derivative. This calculation was conducted in both the x and y directions, and then averaged to find the overall peak radius at that location. Although averaging in the x and y directions may not be the most accurate assumption, it was used to simplify the calculations.

Once the peaks and their radii were determined from the fractal surface, the Hertz contact theory was used to find the contact load vs. displacement relationship. For the present study, a linear contact theory was utilized even if this was a gross approximation. A nonlinear contact theory would be adopted in the next phase of study for more accurate representation of the contact characteristics. As the contact load increased, more peaks became under contact, which meant a larger contact area. The contact area ratio, the actual contact area divided by the nominal contact area, was computed as a function of the contact load or contact displacement.

The thermal conductivity and electric conductivity should be a function of the contact area ratio. As the first order approximation, those conductivities were considered to be linearly proportional to the contact area ratio times those values under perfect contact condition, i.e. perfect bonding without any gap. Those values of conductivities were used at the contact surface between the rail and armature.

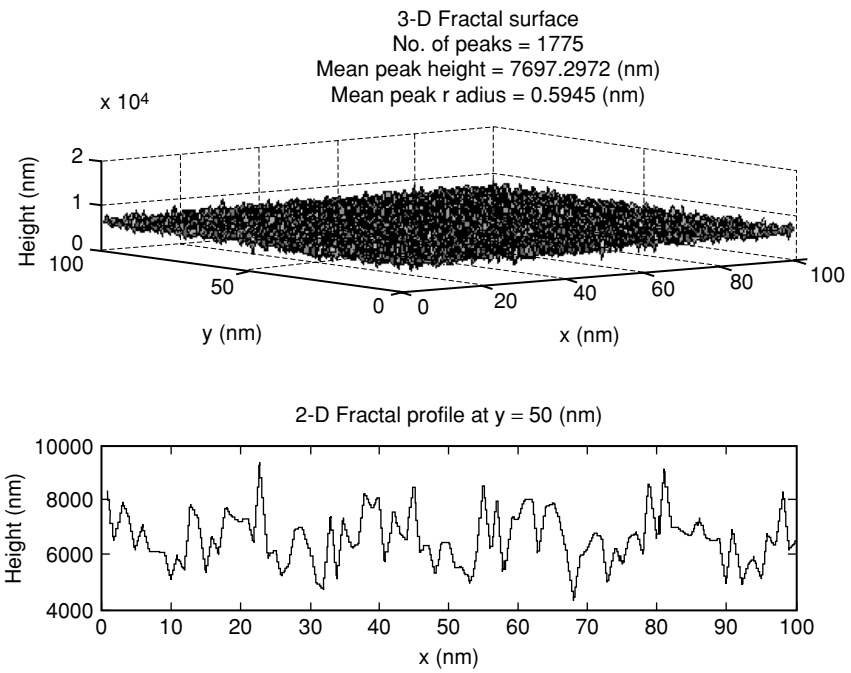

Figure 3 Fractal surface of a nominally flat plane. The top plot is the 3-D view while the bottom plot is a 2-D view with an imaginary cut at y = 50 nm.

4. RESULTS AND DISCUSSION

4.1. CONTACT SURFACE ANALYSIS

Before the rail gun analysis, a parametric study of the fractal surface was undertaken. As the number of superposed fractal ridges, M, in Eq. (15) increased, the total number of peaks as well as the mean peak height increased while the mean peak radius decreased. In other words, peaks became taller and narrower with increasing M. Increasing the number of superposed fractal ridges caused a significant increase in contact pressure. This increase came from an increased number of peaks, thus more peaks in contact. More peaks in contact resulted in a greater contact force, which mean a greater average contact pressure which was calculated for the nominal contact surface area. This result is shown in Fig. 4(a). In addition, more peaks in contact resulted in a larger actual contact area as seen in Fig. 4(b).

The parameter G, called the fractal roughness, in Eq. (15) represents a height scaling parameter. As it falls outside the summations and trigonometric functions in the equation, it is independent of frequency, and affects the results as a mere scale factor. Increasing the fractal roughness simply shifted the surface and profile closer to the x - y plane. The overall number of peaks stayed the same, but the mean peak height decreased. Because the peak height was changed, it had an effect on the peak radius. Thus, the mean peak radius increased, yielding shorter, wider peaks. The increase of G also affected the relationships of contact pressure vs. displacement as well as contact area ratio vs. displacement in a similar way as shown in Fig. 4.

Increasing the fractal dimension, D, slightly increased the number of peaks but decreased the mean peak height with an increase in the mean peak radius. As D is increased, the topography is somewhat smoother, with a narrower frequency band and larger peak radii.

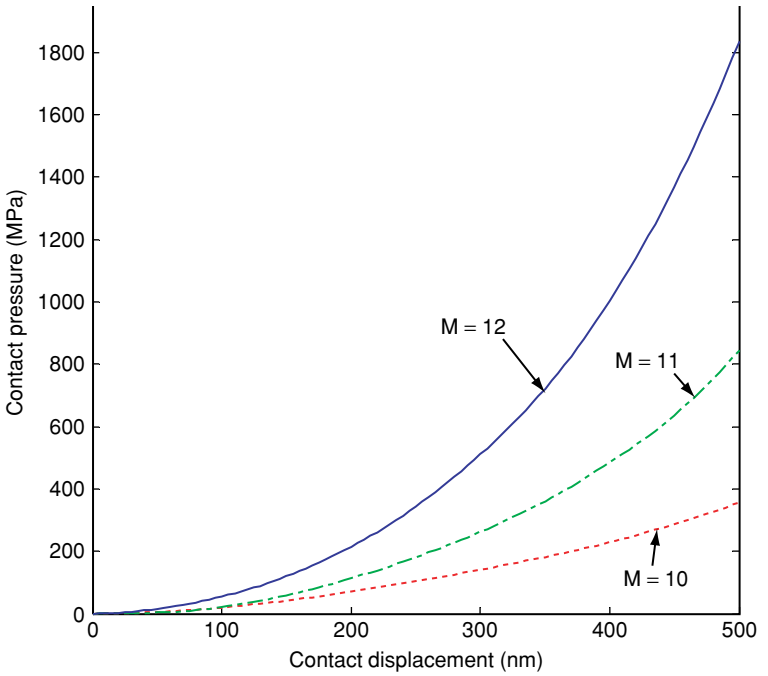

(a) Contact pressure vs. displacement plot

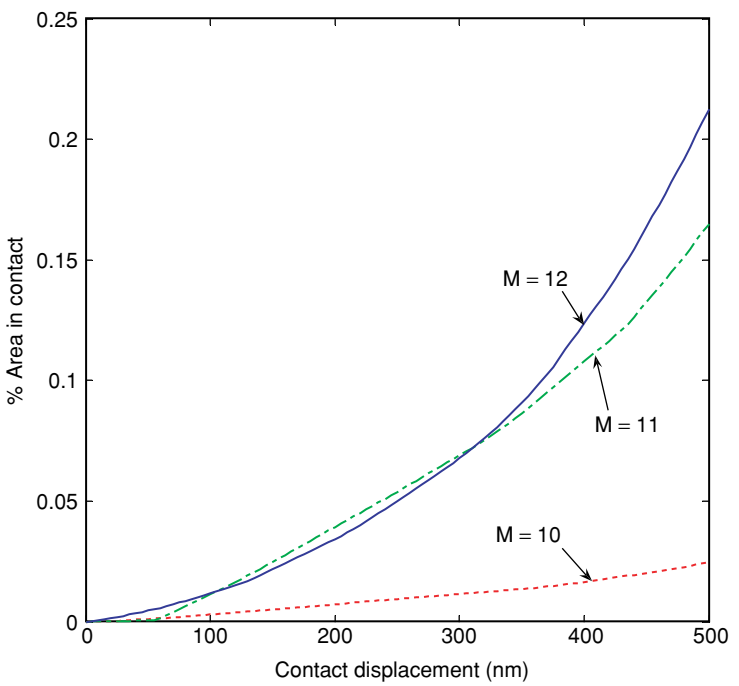

(b) Contact area vs. displacement plot

Figure 4 Variation of *M* in the fractal surface equation.

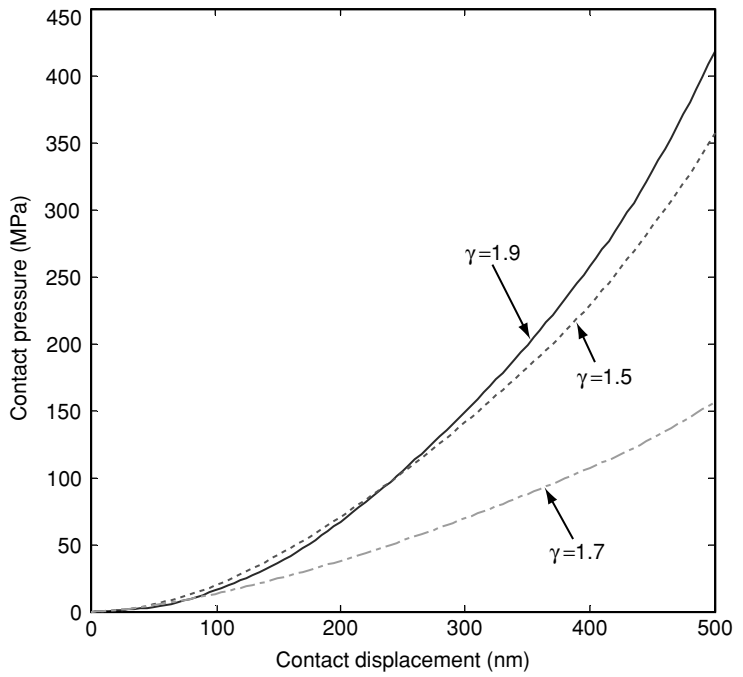

(a) Contact pressure vs. displacement plot

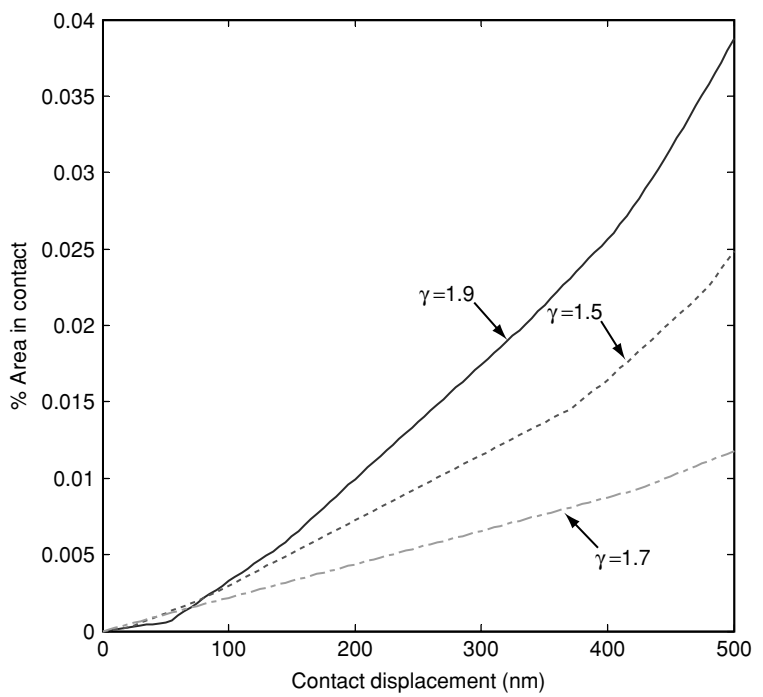

(b) Contact area vs. displacement plot

Figure 5 Variation of γ in the fractal surface equation.

Table 1 Geometric dimensions of rails and armature

Dimensions	Unit (m)
Length of rails	0.5
Width of rails	0.0095
Length of the armature	0.01
Width of the armature	0.019

The effect of D on the contact pressure-displacement and contact area ratio-displacement relationships was qualitatively same as before as plotted in Fig. 4.

However, the parameter γ called the density of the profile frequency had no effect on the number of peaks. The increased γ very slightly decreased the mean peak height and the mean peak radius. As γ was increased, the topography was somewhat smoother, with a narrower frequency band. The peak height distribution was more consistent than that in the baseline, meaning that many of the tall narrow peaks from the baseline had been replaced with shorter, narrower peaks when γ was increased. However, when γ was decreased, it had a greater effect on the profile. The number of peaks was decreased. Decreasing the density of the frequency caused the mean peak height to increase and to decrease the mean peak radius. Thus, the profile was shifted further from the axis, while at the same time the frequency band was decreased when compared to baseline. Overall, the characteristics of the topographical profile was inconsistent for different values of γ. As a result, γ also affected the relationships of contact pressure-displacement and contact area ratio-displacement randomly as shown in Fig. 5.

4.2. RAIL GUN ANALYSIS

A two-dimensional model of a rail gun launcher was investigated, and its geometry was shown in Fig. 6(a), which also shows a finite element mesh. The figure shows two rails and an armature in-between. The armature's shape was simplified as a rectangular shape as shown in the figure. Otherwise, the armature can be modeled as shapes illustrated in Figs. 6(b) and 6(c). The geometric dimensions of the rails and the armature are provided in Table 1. The armature was assumed located initially at 0.01 m from the left with zero initial velocity. An electric potential 6.5 kV was applied to the rails at the initial room temperature of 300 °K. As far as materials are concerned, aluminum, copper, and steel were selected for the present study. Their material properties are available in Ref. [17] so that they are omitted here. The multiphysics-based computations as sketched in Fig. 2 were completed to determine the armature exit velocity and temperature distribution in the rail gun launcher.

In Fig. 7, the aluminum armature velocity is depicted as a function of the distance along three different rail materials; copper, aluminum, and steel. Comparing the results, the copper rails yielded the highest armature velocity. Even if the analysis program already included frictional effect, the friction coefficient was assumed zero for the present study.

The next case switched the rail and armature materials. In other words, copper was used for the armature and aluminum was for rails. Then, this case was compared to the previous case before exchanging the materials in Fig. 8. The aluminum armature/copper rail case resulted in a higher velocity than the opposite combination case. From comparing the values of Lorentz forces which were exerted on the armature, no significant change was observed between the two cases. However, the mass of the aluminum armature was smaller than that of copper because the volume of armature was kept constant in the analysis. The lighter mass of aluminum resulted in a higher velocity from Newton's second law.

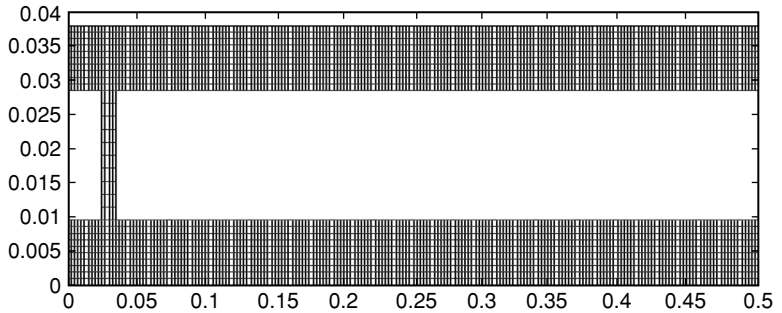

(a) Rectangular shape of solid armature

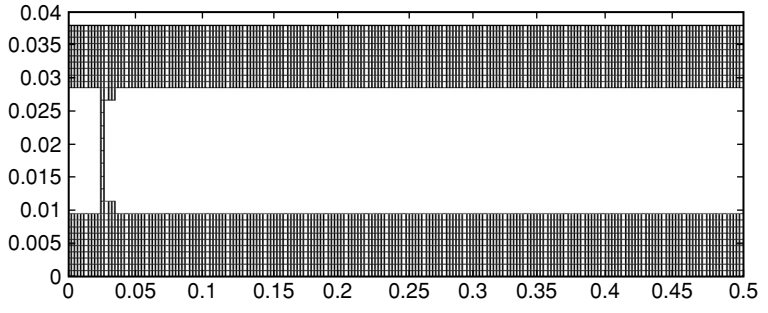

(b) U-shaped solid armature

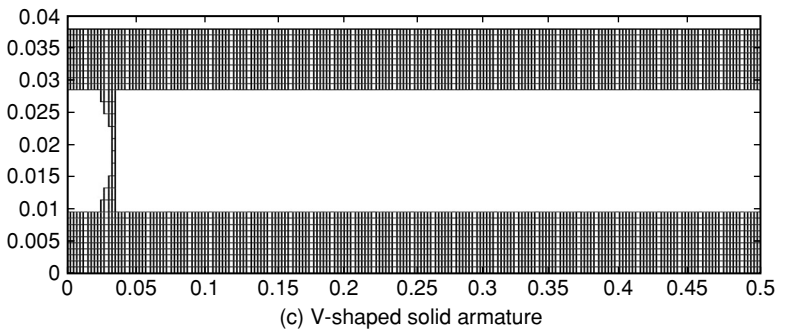

(c) V-shaped solid armature

Figure 6 Finite element mesh of the armature and rails.

However, heat generation and heat transfer were quite different between the two cases, which resulted in very different averages temperatures at the contact interfaces as shown in Fig. 9. The average temperature at the interfaces was lower in the case of copper armature/aluminum rail than that in the opposite material combination case. On the other hand, the former case has a higher rate of temperature rise at the interface as the armature moved along the rail compared to the latter case. In order to further investigate this trend of temperature, the rail was extended to 1 meter long or 1.5 meter long, respectively, for the next study. The results are discussed below.

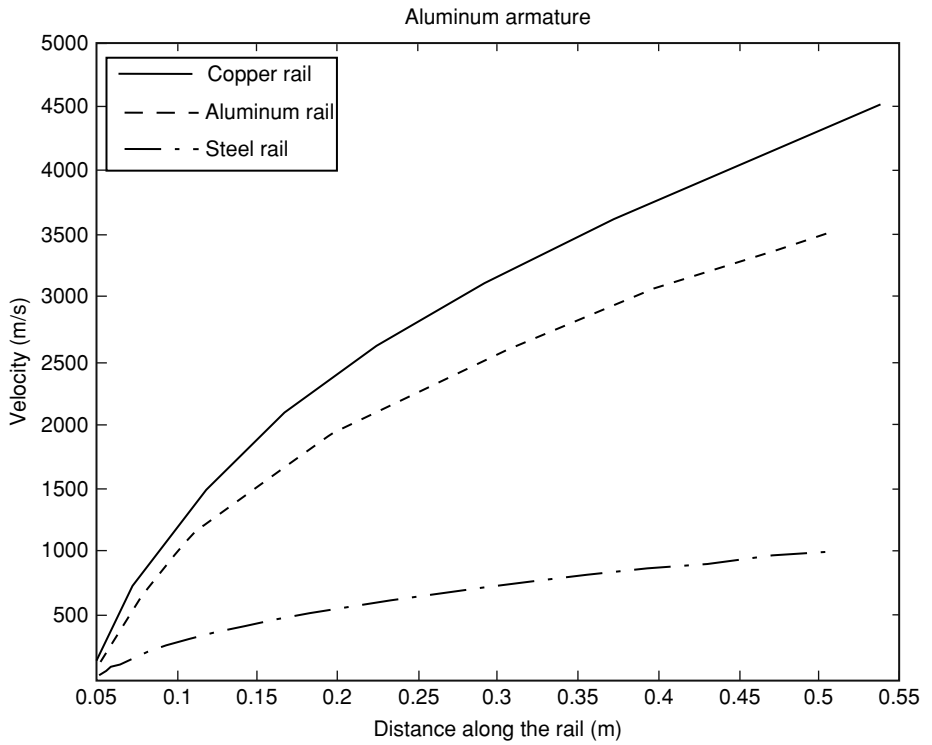

Figure 7 Armature velocity as a function of the distance along the rail for three different rail materials.

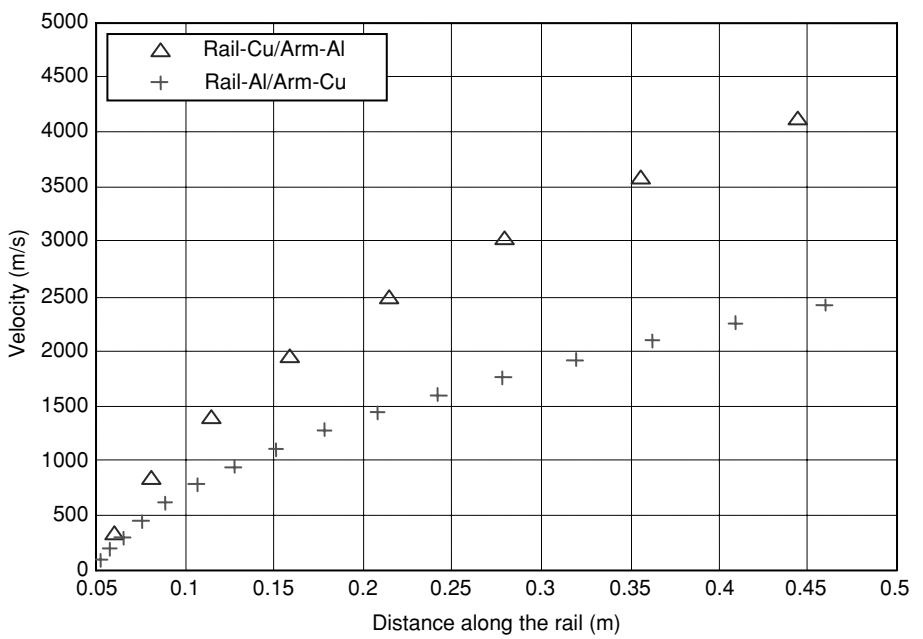

Figure 8 Velocity as a function of the distance along the rail for two different cases of materials.

Table 2 Exit velocities for three different lengths of rails

Exit Velocity	Copper rail/Aluminum armature	Aluminum rail/Copper armature
Barrel length		
0.5 m	4100 m/s	2500 m/s
1.0 m	6200 m/s	3500 m/s
1.5 m	7900 m/s	4500 m/s

Table 3 Kinetic energy for three different lengths of rails

Kinetic Energy	Copper rail/Aluminum armature	Aluminum rail/Copper armature
Barrel length		
0.5 m	82 kJ	100 kJ
1.0 m	188 kJ	198 k
1.5 m	304 kJ	327 kJ

Table 4 Maximum average temperatures at the interfaces

Max. avg. temp.	Copper rail/Aluminum armature	Aluminum rail/Copper armature
Barrel length		
0.5 [m]	760 [°K]	660 [°K]
1 [m]	860 [°K]	920 [°K]
1.5 [m]	1010 [°K]	1430 [°K]

First of all, the velocity was higher for the longer rail as tabulated in Table 2. The increase of the velocity followed a parabolic orbit. Hence, there must be an upper limit at the length of the barrel beyond which any further increase does not significantly affect the value of the exit velocities and makes the design impractical.

Calculation of the kinetic energy from the exit velocity is given in Table 3. It was observed that, the kinetic energy of the aluminum armature was lower than that of the copper one because of its lighter mass. The total mass of the launch object is the mass of the armature and the mass of projectile. That means that the projectile mass can be determined based on either the desired exit velocity or the kinetic energy. Some combination of the two criteria may be also used for designing the weight of the projectile.

Furthermore, of greater interest was what happens at the distribution of the temperature at the interfaces. In Fig. 10, the average temperature at the interfaces is shown as a function of the distance of 1 meter long rail. It can be noticed that there is a point of intersection between the two curves in Fig. 10. Below that point, the average temperature at the interfaces is lower for the copper armature than that of aluminum armature. After that point, the state is reversed. The maximum values of average temperatures for the two cases are shown in Table 4.

Two questions now arose. Why was the initial average temperature of the aluminum armature case higher than that of the copper armature case, and why the rate of increase of the former was lower than that of the latter?

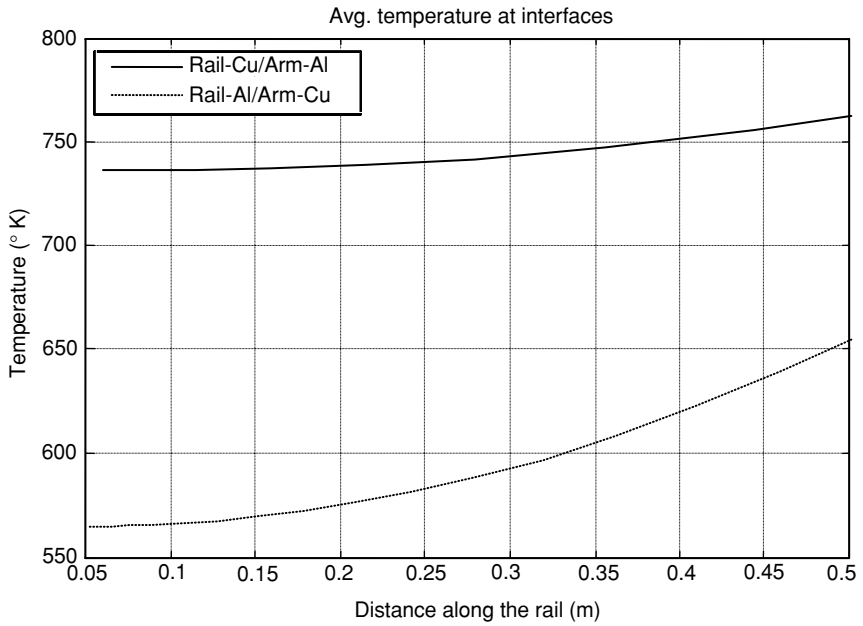

Figure 9 Average temperatures at the interface between the rails and the armature for two different material combinations.

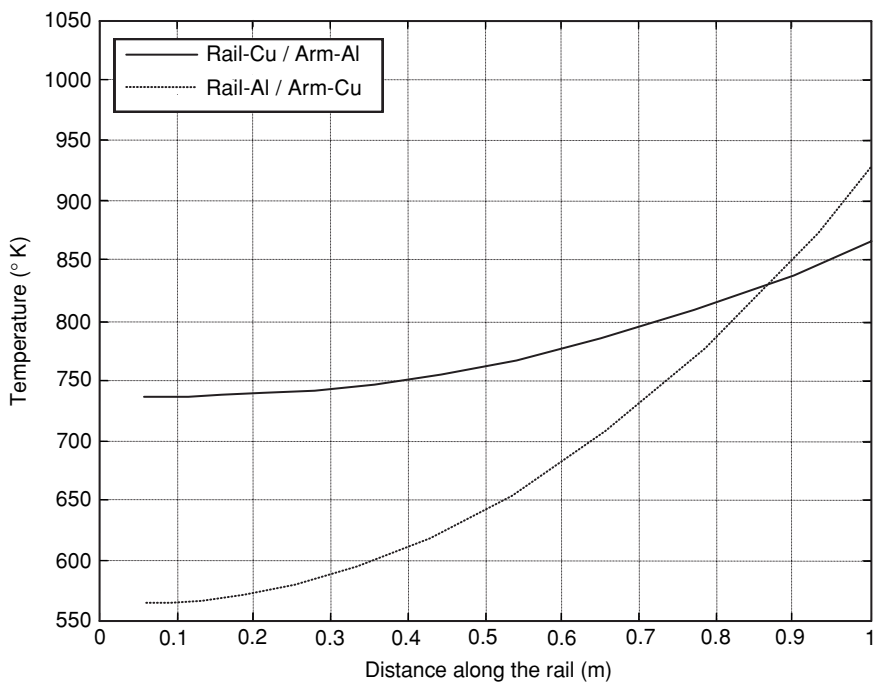

Figure 10 Average temperatures at the interface between the 1 m long rails.

Taking into consideration of the specific design which we have selected, initially the area conducting electricity of the armature is larger than that of the two rails because the armature was positioned very close to the edge of the rails through which electricity flows. In addition, aluminum has a higher value of electric resistivity than that of copper. That means initially the total electric resistance of the system is higher for the aluminum armature case than that of the copper armature case. This resulted in a larger amount of heat in the former case than in the latter case. This is the reason why initially the aluminum armature case has a higher interface temperature profile.

As long as the armature goes down the rails, the total resistance is increased with the traveled distance along the rails. In the case of copper rails, a lower electric resistivity is added, whereas in the case of aluminum rails a higher resistivity is added. This causes the release of a lower amount of heat in the copper rail/aluminum armature case than in the opposite combination case. Furthermore, taking into consideration the values of thermal conductivities of the two materials (copper has a higher thermal conductivity than aluminum), the copper rail/aluminum armature case has not only a lower amount of heat generation but also a higher dissipation of heat with a higher thermal conductivity of the copper rail. For these reason the rate of increase of the temperature profile at the interfaces is lower for this case.

5. CONCLUSIONS

In this paper, a multiphysics-based computer program was developed for calculating the exit velocity, acceleration, Lorentz force, temperature, and stress distribution of a rail gun launcher. The analysis modules included electromagnetic field analysis, Lorentz force calculation, Joule's heat calculation, transient heat conduction analysis, thermal stress analysis, and dynamic analysis of the armature. In particular, the armature/rail interface properties, like electric and thermal conductivities, were estimated based on a fractal contact model, and those values were used in this work.

The study showed that there was a upper limit of the length of the barrel of the rail gun beyond that point the increase in length did not increase the exit velocity any longer. Furthermore, a study was conducted for different constructive materials in order to investigate and explain their different characteristics. Some physical explanations were provided for the behaviors observed from different combinations of materials for the armature and rails.

The developed computer modeling and simulation tool would be useful for design of a rail gun considering various input parameters. The present model was for 2-D analysis, but it can be extended to 3-D analysis. In addition, the subsequent study will consider more advanced interface model for electric and thermal conductivities.

REFERENCES

[1] H. D. Fair, "Electromagnetic propulsion: a new initiative", *IEEE Transactions on Magetics,* Vol. Mag-18, No. 1, pp. 4–6, January 1982.

[2] J. D. Powell, "Thermal-energy transfer from arc to rails in an arc-driven rail gun", *IEEE Transactions on Mangnetics*, Vol. Mag-20, No. 2, pp. 395–398, March 1984.

[3] S. P. Atkinson, "The use of finite element analysis techniques for solving rail gun problems", *IEEE Transactions on Magnetics*, Vol. 25, No. 1, pp. 52–56, January 1989.

[4] D. Rodger and P. J. Leonard, "Modeling the electromagnetic performance of moving rail gun launchers using finite elements", *IEEE Transactions on Magnetics,* Vol. 29, No. 1, pp. 496–498, January 1993.

[5] I. Kohlberg and W. O. Coburn, "A solution for the three dimensional rail gun current distribution and electromagnetic fields of a rail launcher", *IEEE Transactions on Magnetics*, Vol. 31, No.1, pp. 628–633, January 1995.

[6] S. Barmada, A. Musolino, M. Raugi, and R. Rizzo, "Numerical simulation of a complete generator-rail launch system", *IEEE Transactions on Magnetics*, Vol. 41, No. 1, pp. 369–374, January 2005.

[7] O. Biro and K. Preis, "On the use of magnetic vector potential in the finite element analysis of three-dimensional eddy currents", *IEEE Transactions on Magnetics*, Vol. 25, No. 4., pp. 3145–3159, July 1989.

[8] K. Muramatsu, T. Nakata, T. Takahashi, and K. Fuhiwara, "Comparison of coordinate systems for eddy current analysis in moving conductors", *IEEE Transactions on Magnetics*, Vol. 28, No. 2, pp. 1186–1189, March 1992.

[9] K.-T. Hsieh, "A Lagrangian formulation for mechanically, thermally coupled electromagnetic diffusive processes with moving conductors", *IEEE Transactions on Magnetics*, Vol. 31, No. 1, pp. 604–609, January 1995.

[10] A. Nysveen and R. Nilssen, "Time domain simulation of magnetic systems with a general moving geometry", *IEEE Transactions on Magnetics*, Vol. 33, No. 2, pp. 1394–1397, March 1997.

[11] J.-F. Lee, R. Lee, and A. Cangellaris, "Time-domain finite-element method", *IEEE Transactions on Antennas and Propagation*, Vol. 45, No. 3, pp. 430–442, March 1997.

[12] C. S. Biddlecombe, J. Simkin, A. P. jay, J. K. Sykulski, and S. Lepaul, "Eletromagnetic analysis coupled to electric circuits and motion", *IEEE Transactions on Magnetics*, Vol. 34, No. 5, pp. 3182–3185, September 1998.

[13] D.-H. Kim, S.-Y. Hahn, I.-H. Park, and G. Cha, "Computation of three-dimensional electromagnetic field including moving media by indirect boundary integral equation method", *IEEE Transactions on Magnetics*, Vol. 35, No. 3, pp. 1932–1938, May 1999.

[14] T. Iwashita and M. Shimasaki, "Parallel processing of 3-D eddy current analysis with moving conductor using parallelized ICCG solver with renumbering process", *IEEE Transactions on Magnetics*, Vol. 36, No. 4, pp. 1504–1509, July 2000.

[15] Y. W. Kwon and H. Bang, *The Finite Element Method Using MATLAB*, 2nd ed., CRC Press, Boca Raton, 2000.

[16] W. Yan and K. Komvopoulos, "Contact Analysis of Elastic-Plastic Fractal Surfaces," *Journal of Applied Physics*, Vol. 84, No. 7 (Oct. 1, 1998), pp. 3617–3624.

[17] MatWeb website. http://www.matweb.com/search/GetProperty.asp